Na-induced n-to-p-type conversion and thermoelectric properties of the layered oxysulfide $LaOBiPb_{1-x}Na_xS_3$

Yi Yu,[1,*] Chao Cheng,[2] Youmin Guo,[1] and Chunchang Wang[1]

[1]*School of Material Science and Engineering, Anhui University, Hefei 230601, China*

[2]*Institute of Physical Science and Information Technology, Anhui University, Hefei 230601, China*

Abstract

The electrical transport and thermoelectric properties of Na-doped $LaOBiPbS_3$ are systematically investigated. Na substitution at the Pb site acts as an effective acceptor, converting the carrier type from n-type to p-type, as evidenced by a well-defined compensation point near $x = 0.04$ where the resistivity peaks and the Hall coefficient changes sign. The optimal p-type composition $LaOBiPb_{0.94}Na_{0.06}S_3$ delivers a power factor of 5.45 $\mu W\,cm^{-1}\,K^{-2}$ and a maximum ZT of 0.33 at 773 K, reaching 3.2 and 2.5 times the PF and ZT values of the parent compound, respectively. For the heavily doped $x = 0.08$ sample, a simultaneous anomaly in resistivity and Seebeck coefficient emerges above 600 K, ascribed to the interplay of bipolar conduction and local lattice strain induced by excessive Na incorporation. These findings establish Na doping as an effective strategy for realizing p-type conductivity and enhancing thermoelectric performance in this layered oxysulfide system.

PACS numbers: 74.25.F-, 74.62.En, 74.20.Rp, 74.70.Xa

Keywords: $LaOBiPb_{1-x}Na_xS_3$; n-to-p-type conversion; thermoelectric properties; Pisarenko analysis

*To whom correspondence should be addressed. Email address: onlyyuyi@mail.ustc.edu.cn

I. INTRODUCTION

Thermoelectric materials, capable of direct interconversion between heat and electricity, hold great promise for solid-state refrigeration and waste-heat recovery[1, 2]. The conversion efficiency is governed by the dimensionless figure of merit $ZT = S^2T/\rho\kappa$, where S, T, ρ and κ denote the Seebeck coefficient, temperature, electrical resistivity, and total thermal conductivity, respectively. Achieving high thermoelectric performance thus requires a combination of large power factor $PF = S^2/\rho$ and low thermal conductivity. Layered $LnOBiS_2$ compounds (Ln = rare earth) have attracted considerable interest owing to their "phonon-glass electron-crystal" nature and high tunability. While the parent phase is insulating, the carrier concentration can be effectively modulated via anionic or cationic substitution[3–5]. For instance, F-doping and Se-substitution in $LaOBiS_2$ have concurrently optimized the power factor and suppressed the lattice thermal conductivity, achieving a maximum ZT of approximately 0.36 at 650 K[6, 7]. To further lower the thermal conductivity and improve the thermoelectric performance, a PbS-type layer was intercalated into the van der Waals gap of $LaOBiS_2$, forming the quaternary compound $LaOBiPbS_3$ (space group $P4/nmm$)[8, 9]. This natural superlattice structure features a quasi-two-dimensional electronic structure favorable for thermoelectric transport[10]. N-type carrier doping was successfully achieved through F substitution for O, enhancing the PF by 30% at 770 K and demonstrating the potential of this material system[11].

Despite these advances, thermoelectric exploration of $LaOBiPbS_3$ has largely been confined to n-type doping. For practical device applications, however, high-performance p-type counterparts are equally indispensable yet remain exceedingly rare. The scarcity arises because common acceptor dopants such as Cu and Ag tend to intercalate into the van der Waals gap rather than occupying cation sites, often leading to over-doping and metallic-like behavior[12]. Sodium, a monovalent alkali metal with a six-coordinate ionic radius of 1.02 Å, which is smaller than that of Pb^{2+} (1.19 Å), is expected to preferentially occupy the Pb site and act as a controlled acceptor dopant. Indeed, Na doping has been demonstrated to effectively introduce holes and convert n-type PbS into a p-type thermoelectric material with a high ZT[13]; similar doping strategies were also successful in PbSe/PbTe systems[14–16]. However, a systematic investigation of Na substitution at the Pb site in $LaOBiPbS_3$, together with its influence on the crystal structure, electronic transport, and thermoelectric

figure of merit, has not been reported to date.

In this work, we report the synthesis and thermoelectric properties of Na-doped $LaOBiPbS_3$ polycrystalline samples. It is demonstrated that a small amount of Na substituted for Pb ($x \leq 0.08$) can gradually switch the majority carrier type from electrons to holes, accompanied by continuous evolution of the transport coefficients. Through optimization of the Na concentration followed by hot-pressing and annealing treatments, a competitive p-type ZT is achieved. The results highlight the feasibility of Na doping as a viable route toward p-type $LaOBiPbS_3$-based thermoelectrics.

II. EXPERIMENT

Polycrystalline samples of $LaOBiPb_{1-x}Na_xS_3$ (x = 0, 0.02, 0.04, 0.06, 0.08) were synthesized by a solid-state reaction method. High-purity starting powders, comprising La_2S_3 (99%), La_2O_3 (99.99%), Bi_2S_3 (99%), PbS (99.9%), anhydrous Na_2S (99.9%), and sublimed sulfur (99.99%), were weighed according to the stoichiometric ratios. To compensate for sulfur evaporation during high-temperature sintering, an additional 5% of sulfur powder (relative to the total mass of starting materials) was added to the mixture. All manipulations were performed inside an argon-filled glove box where the H_2O and O_2 levels remained below 1 ppm. The weighed powders were ground thoroughly in an agate mortar, pressed into pellets under a uniaxial pressure of 10 MPa, and sealed in evacuated quartz tubes at pressures below 2×10^{-5} Pa. The sealed tubes were heated to 700 °C at 2 °C/min, held for 24 h, and furnace-cooled. The resulting ingots were reground, pelletized again, and sintered at 750 °C for 48 h under the same vacuum conditions to obtain single-phase powder. This powder was loaded into a graphite die and consolidated via vacuum hot pressing at 650 °C for 45 min under a uniaxial pressure of 50 MPa. The resulting bulk specimens were then sealed in evacuated quartz tubes and annealed at 550 °C for 12 h. All transport measurements were performed on specimens cut along the same direction from the hot-pressed pellets, i.e., perpendicular to the uniaxial pressing direction, so that the electrical and thermal transport properties were probed along the same crystallographic orientation. No porosity correction was applied to the measured transport data. The final specimens exhibited a relative density of approximately 92%, calculated from the unit-cell parameters obtained in powder XRD data.

Powder X-ray diffraction (XRD) patterns were recorded at room temperature using a Rigaku SmartLab diffractometer. The chemical states and surface compositions were analyzed by X-ray photoelectron spectroscopy (XPS) using an ESCALAB 250Xi spectrometer (Thermo Fisher Scientific, USA). Electrical resistivity at low temperatures was measured on bar-shaped specimens (typical dimensions: $3 \times 2 \times 0.5\,\mathrm{mm}^3$) by a standard four-probe method using a Quantum Design Physical Properties Measurement System (PPMS) over a temperature range of 2–300 K. Hall coefficients were also acquired in the PPMS; prior to the Hall measurements, the samples were carefully polished to a thickness of approximately 0.1 mm to minimize geometric uncertainties. Simultaneous high-temperature resistivity and Seebeck coefficient data were collected from 300 to 773 K on a commercial apparatus (ZEM-3, Advance Riko, Japan) under a low-pressure helium atmosphere. The thermal conductivity κ was calculated using the equation $\kappa = \lambda C_p d$, where λ and C_p represent the thermal diffusivity and specific heat capacity, respectively, measured via a NETZSCH LFA 467 laser flash apparatus under an argon atmosphere. The geometric density d was determined using the Archimedes method.

The Pisarenko plot was constructed using a single parabolic band (SPB) model under the degenerate approximation, $S = (8\pi^2 k_B^2/(3eh^2))\, m^* T\, (\pi/(3n))^{2/3}$, assuming acoustic phonon scattering, a rigid band, and a degenerate carrier distribution. The effective masses obtained by fitting the experimental data to this expression are $0.082\, m_e$ and $0.178\, m_e$ for the n-type and p-type samples, respectively. The carrier concentrations were derived from Hall measurements using $n_H = 1/(e|R_H|)$ under the single-carrier approximation. The lattice thermal conductivity κ_L was obtained by subtracting the electronic contribution from the measured total thermal conductivity, $\kappa_L = \kappa - LT/\rho$, where the electronic term follows the Wiedemann–Franz law. A degenerate Lorenz number $L = 2.44 \times 10^{-8}\ \mathrm{W\,\Omega\,K^{-2}}$ was adopted for all samples, assuming acoustic-phonon-dominated scattering in the strongly degenerate limit.

III. RESULTS AND DISCUSSION

Figure 1 presents the room-temperature powder X-ray diffraction (XRD) patterns of $\mathrm{LaOBiPb_{1-x}Na_xS_3}$ ($x = 0, 0.02, 0.04, 0.06, 0.08$). All diffraction peaks for $x \leq 0.06$ can be indexed to the tetragonal P4/nmm space group (No. 129), consistent with the parent

$LaOBiPbS_3$ layered structure, indicating the successful incorporation of Na dopants into the Pb sublattice without forming long-range ordered secondary phases. For the $x = 0.08$ sample, two additional weak reflections appear around 39.0° and 46.0°, which are assigned to the (220) and (311) reflections of cubic Na_2S, respectively. This indicates that the solubility limit of Na at the Pb site is approached or exceeded near $x = 0.08$. No discernible shift of the principal diffraction peaks was observed with increasing Na concentration. Considering the six-coordinate ionic radii of Na^+ (1.02 Å) and Pb^{2+} (1.19 Å), Na substitution is expected to cause a slight lattice contraction. However, the effect is below the resolution of our laboratory XRD for the low doping levels studied here. In addition, for the $x = 0.08$ sample, the formation of a minor Na_2S impurity phase consumes part of the Na, further reducing the amount incorporated into the Pb site. These factors account for the absence of a detectable peak shift. In addition, no pronounced preferred orientation was observed in the XRD patterns; the relative intensities of the diffraction peaks are consistent with those of a randomly oriented powder standard, indicating that the hot-pressed samples are essentially free of texture. Meanwhile, moderate peak broadening is observed, suggesting enhanced microstrain and compositional fluctuations induced by aliovalent substitution. Notably, the intensity ratio of the (006) to the (103) reflection exhibits a non-monotonic trend, increasing up to $x = 0.04$ and subsequently declining at higher doping levels. Although the precise origin of this behavior requires further elucidation, it likely reflects a redistribution of electron density along the c-axis, analogous to that reported in F-doped $LaOBiPbS_3$[10].

X-ray photoelectron spectroscopy (XPS) was employed to investigate the surface chemical composition. Due to the inherent limitations of XPS in quantifying light elements, oxygen is omitted from the quantitative analysis. Table I compares the nominal and XPS-derived compositions, with the Bi content normalized to 1.00. The XPS results confirm the successful incorporation of Na into the lattice, as the measured Na content increases monotonically with the nominal doping level. The sulfur content is systematically underestimated relative to the stoichiometric value, despite the use of a 5 wt% sulfur excess during synthesis. Since no Ar^+ etching was performed in this work, the apparent sulfur deficiency should be considered primarily as a surface artifact arising from the oxidation of sulfide to sulfate and the partial desorption of SO_2 under ultrahigh vacuum. Similar surface sulfur depletion has been widely reported in XPS studies of layered sulfides, while the bulk sulfur stoichiometry is typically preserved. Indeed, the powder XRD patterns (Fig. 1) show no impurity phases related

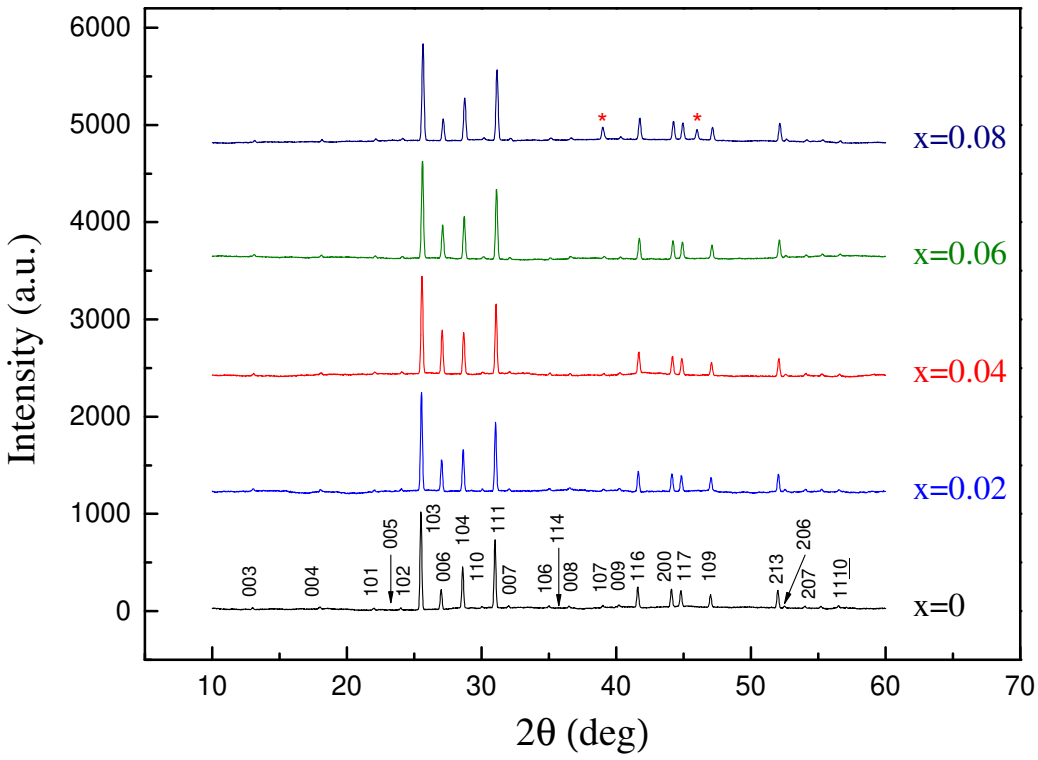


FIG. 1: (color online) Powder x-ray diffraction patterns for the $LaOBiPb_{1-x}Na_xS_3$ ($x = 0 - 0.08$) samples. Reflections of extra impurities are marked by the red asterisks.

to sulfur deficiency for $x \leq 0.06$, and the lattice parameters remain essentially unchanged, supporting a near-stoichiometric bulk composition. The Pb content is slightly lower than the nominal composition, which can be attributed to minor Pb loss during high-temperature sintering and surface oxidation. It should be noted that XPS probes only the outermost surface layers, and the bulk composition was not independently verified by ICP in this work. Nevertheless, the transport data provide strong indirect evidence for the incorporation of Na as an acceptor: the Hall coefficient changes sign from negative to positive with increasing Na content, and the carrier concentration evolves systematically with x, consistent with the XPS-derived Na contents. These observations confirm that Na is successfully doped into the lattice and governs the bulk electrical transport, while the sulfur deficiency is predominantly a surface effect.

Figure 2(a) shows the temperature-dependent resistivity $\rho(T)$ of the $LaOBiPb_{1-x}Na_xS_3$

TABLE I: Comparisons between the nominal and XPS-derived compositions of the $LaOBiPb_{1-x}Na_xS_3$ samples

Nominal composition	XPS-derived composition
$LaOBiPbS_3$	$La_{1.05\pm0.04}OBiPb_{0.98\pm0.02}S_{2.89\pm0.10}$
$LaOBiPb_{0.98}Na_{0.02}S_3$	$La_{1.05\pm0.05}OBiPb_{0.96\pm0.02}Na_{0.03\pm0.01}S_{2.85\pm0.12}$
$LaOBiPb_{0.96}Na_{0.04}S_3$	$La_{1.05\pm0.03}OBiPb_{0.95\pm0.03}Na_{0.04\pm0.01}S_{2.81\pm0.10}$
$LaOBiPb_{0.94}Na_{0.06}S_3$	$La_{1.06\pm0.05}OBiPb_{0.92\pm0.03}Na_{0.06\pm0.02}S_{2.79\pm0.15}$
$LaOBiPb_{0.92}Na_{0.08}S_3$	$La_{1.03\pm0.04}OBiPb_{0.90\pm0.04}Na_{0.08\pm0.01}S_{2.78\pm0.15}$

($x = 0-0.08$) polycrystals from 2 to 300 K. The parent compound, previously identified as an n-type semiconductor through Hall and Seebeck measurements[11], exhibits semiconducting behavior throughout the measured range. Upon light Na doping ($x = 0.02$), the low-temperature resistivity rises substantially, roughly tripling at 2 K. The resistivity reaches a maximum at $x = 0.04$. Heavier doping causes drastic suppression of ρ. As displayed in the inset, the 2 K resistivity drops by 3–4 orders of magnitude. The non-monotonic transport evolution is attributed to the compensation of intrinsic electrons by Na-induced holes. At low doping levels, the net carrier density decreases, giving rise to a marked increase in ρ. The electron and hole concentrations become comparable near $x = 0.04$, forming a compensation point. Further introduction of holes at $x = 0.06$ and 0.08 renders the p-type conduction predominant, leading to a dramatic drop in ρ by several orders of magnitude. A subtle resistivity hump is observed around 15–20 K for $x = 0.06$, while for $x = 0.08$ only a barely discernible downward curvature appears at the lowest temperatures. Similar anomalies, coupled with a peak in the Seebeck coefficient, have been reported in F-doped $LaOBiPbS_3$ and attributed to phase competition or, more specifically, to a nontrivial electronic structure arising from intrinsic non-stoichiometry of the system[11, 17].

To directly verify the carrier type evolution, variable-temperature Hall measurements were performed. Figure 2(b) displays the temperature dependence of the Hall coefficient R_H over the range of 2–380 K. The parent compound exhibits a negative R_H across the entire temperature range, with the magnitude increased by a factor of 3 upon cooling. This moderate temperature dependence suggests that the parent phase lies near the degenerate–nondegenerate boundary, with a high intrinsic carrier concentration but still detectable

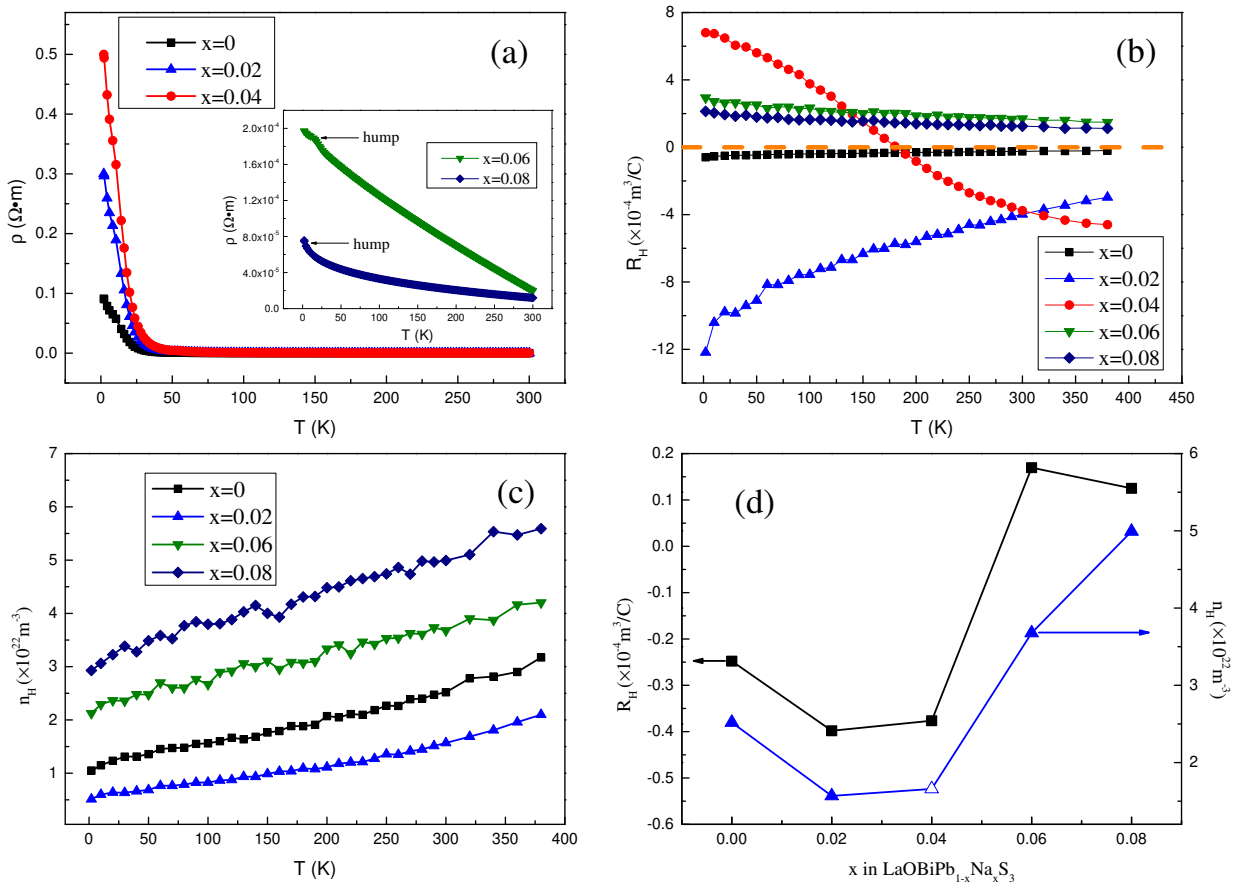


FIG. 2: (color online) (a) Temperature-dependent resistivity $\rho(T)$ of $LaOBiPb_{1-x}Na_xS_3$ ($x = 0 - 0.04$) samples from 2 to 300 K. The inset displays the $\rho(T)$ for $x = 0.06$ and 0.08. (b) Hall coefficient R_H as a function of temperature over 2–380 K. The gold dashed line marks $R_H = 0$, serving as a guide for the sign reversal. (c) Nominal carrier concentration n_H derived from the Hall data. The curve for $x = 0.04$ is omitted as the single-carrier approximation breaks down near the compensation point. (d) Composition dependence of R_H and n_H at 300 K, the open symbol for $x = 0.04$ indicates limited reliability of the single-carrier analysis. The colored arrows are guides for the eyes, pointing to the corresponding coordinates.

carrier freeze-out at low temperatures. For $x = 0.02$, R_H remains negative but shows a stronger temperature dependence, indicating a reduction in the net electron concentration due to partial compensation. At $x = 0.04$, R_H changes sign from positive at low temperatures to negative above 175 K, showing a clear signature of mixed electron–hole conduction near the compensation point. Both $x = 0.06$ and 0.08 samples display positive R_H over the whole measured range with only a weak temperature variation. Combined with the low

resistivity values of these two samples in Fig. 2(a), the weak temperature dependence of R_H indicates that the system has entered a degenerate p-type conduction regime, albeit with a residual carrier freeze-out effect.

Figure 2(c) presents the nominal carrier concentration $n_H = 1/(e|R_H|)$ as a function of temperature under the single-carrier approximation, where e is the absolute value of the electron charge. The data for $x = 0.04$ are omitted, as both electrons and holes contribute significantly to conduction near the compensation point and the single-band approximation breaks down. In this regime, the actual carrier concentrations are more appropriately described by a two-carrier model. For the other compositions, n_H reflects the evolution of the majority carrier density: the values for $x = 0.02$ are lower than those of the parent compound due to electron compensation, while those for $x = 0.06$ and 0.08 progressively decrease as hole doping increases, consistent with the R_H results.

Figure 2(d) summarizes the composition dependence of R_H and n_H at 300 K. The Hall coefficient increases monotonically from negative to positive with increasing x, crossing zero near $x = 0.04$. The sign reversal provides unambiguous evidence for the transition from n-type to p-type conduction. The nominal carrier concentration n_H decreases upon light doping, reaches a minimum, and then rises with further Na substitution, peaking at $x = 0.08$. This trend mirrors the evolution of the net carrier density across the compensation regime. It is worth noting that although R_H is negative at 300 K for $x = 0.04$, the single-carrier approximation is still influenced by the residual hole contribution and may overestimate the true electron density. Hence, the data point for $x = 0.04$ is plotted with an open symbol. Collectively, these results demonstrate that Na substitution at the Pb site acts as an effective acceptor, enabling systematic control of both the type and density of charge carriers in $LaOBiPbS_3$.

Figure 3(a) displays the temperature dependence of resistivity for the $LaOBiPb_{1-x}Na_xS_3$ samples from 300 to 773 K. The parent sample displays a weak metallic upturn, consistent with a weakly degenerate n-type semiconductor with Fermi level lying close to the conduction band edge. For the compensated samples ($x = 0.02, 0.04$), ρ decreases with increasing temperature, reflecting the thermal activation of carriers in the non-degenerate regime. In the inset, the resistivity of the $x = 0.06$ sample increases modestly over the whole temperature range, showing degenerate conduction with residual impurity scattering. On an expanded scale (main panel), ρ of this sample appears nearly temperature-independent.

Notably, the heavily doped $x = 0.08$ sample displays a broad hump centered around 690 K, which is absent in the $x = 0.06$ sample. A similar high-temperature anomaly was reported in heavily F-doped $LaOBiPbS_3$[11], and is generally attributed to a local lattice instability or dynamic phase separation arising from over-doping. For the present $x = 0.08$ sample, however, the XRD pattern reveals a minor Na_2S impurity phase (Fig. 1), which may also contribute to the anomaly. Therefore, the observed hump is attributed to the combined effects of the Na_2S impurity phase and local lattice instability, and further investigation is required to clarify the exact mechanism. The markedly weaker hump amplitude in the Na-doped samples compared to the F-doped ones suggests that Na substitution at the Pb site induces less structural perturbation.

The absolute Seebeck coefficient $|S|$ as a function of temperature is plotted in Fig. 3(b). The parent and lightly doped samples ($x = 0.02, 0.04$) exhibit negative Seebeck coefficients (n-type), while $x = 0.06$ and 0.08 show positive values (p-type), confirming the carrier-type conversion observed in Hall measurements. For the optimized p-type sample ($x = 0.06$), $|S|$ increases steadily from 65 μV/K at 300 K to 115 μV/K at 773 K. This pronounced temperature dependence, while still consistent with degenerate semiconductor behavior, yields a notably high Seebeck coefficient at elevated temperatures, which is beneficial for high-temperature thermoelectric performance. The $x = 0.08$ sample exhibits a similar trend, reaching $\sim$103 μV/K at 773 K, but with a small hump near 690 K that mirrors the resistivity anomaly, further supporting a temperature-induced modification of the electronic structure.

To obtain deeper insight into the band structure, a room-temperature Pisarenko plot of $|S|$ versus the Hall-derived carrier concentration $n_H = 1/(e|R_H|)$ (single-band equivalent) is shown in Fig. 3(c). The data are compared with single-parabolic-band (SPB) curves calculated in the degenerate limit assuming acoustic-phonon scattering. The n-type compositions ($x = 0$, 0.02) are well described by an SPB curve with $m^* = 0.082\mathrm{m}_e$, whereas the p-type compositions ($x = 0.06$, 0.08) yield $m^* = 0.178\mathrm{m}_e$. The somewhat larger effective mass for holes may reflect a flatter valence band or a larger band degeneracy; distinguishing these scenarios requires explicit band-structure calculations. Crucially, the data point near the compensation point ($x = 0.04$) falls significantly below both SPB branches. While this deviation is consistent with a weak bipolar contribution at 300 K[18], the gradual increase of $|S|$ with temperature for the $x = 0.04$ sample (Fig. 3(b)) shows that strong bipolar conduction does not develop within the measured range; the suppression of $|S|$ at the com-

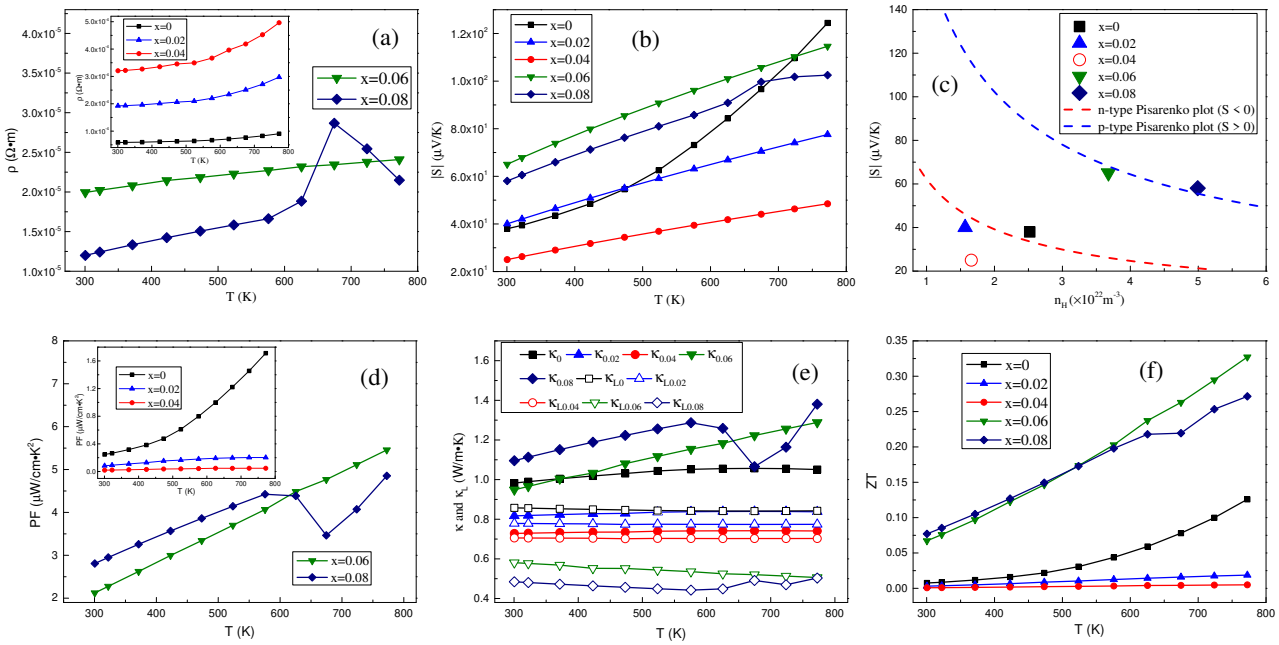


FIG. 3: (color online) High-temperature thermoelectric properties of $LaOBiPb_{1-x}Na_xS_3$ ($x = 0 - 0.08$). (a) Temperature dependence of the resistivity for $x = 0.06$ and 0.08 from 300 to 773 K, plots for $x = 0 - 0.04$ are in the inset. (b) Temperature dependence of the absolute Seebeck coefficient $|S|$ from 300–773 K. (c) Room-temperature Pisarenko plot: $|S|$ versus Hall-derived carrier concentration n_H. The dashed lines in different colors represent single parabolic band (SPB) curves for p-type and n-type carriers with different effective masses, respectively; see the Experiments section for the formula and fitting parameters. The data point for $x = 0.04$ is shown with an open symbol, as it fails to fit into either curve. Temperature dependence of the (d) power factor PF, (e) total thermal conductivity κ (solid symbols) and lattice thermal conductivity κ_L (open symbols), (f) dimensionless figure of merit ZT from 300–773 K.

pensation point thus likely reflects combined weak bipolar effects and the limited accuracy of the single-band parabolic approximation near the carrier-type crossover. Within the n- and p-type branches, the agreement with branch-specific fixed effective masses indicates

that Na doping mainly tunes the carrier concentration, without significantly altering the density-of-states effective mass near the Fermi level.

The power factor PF is presented in Fig. 3(d). The parent sample shows a modest PF of 1.71 μW cm^{-1} K^{-2} at 773 K, limited by its relatively high resistivity. The compensated samples ($x = 0.02, 0.04$) exhibit even lower PF due to their elevated resistivity. In the p-type region, PF increases dramatically, as the $x = 0.06$ sample reaches a maximum of 5.45 μW cm^{-1} K^{-2} at 773 K, outperforming the optimum n-type counterparts in this system. This enhancement arises from the simultaneous optimization of electrical conductivity and Seebeck coefficient upon crossing the compensation point. The $x = 0.08$ sample exhibits a slightly reduced PF, partly due to the high-temperature resistivity anomaly and a marginally lower Seebeck coefficient. The PF reaches 3.2 times that of the parent compound, far exceeding the modest 1.3-fold value reported for F-doped $LaOBiPbS_3$[11], demonstrating that Na doping is an effective route to high-performance p-type thermoelectrics in this layered oxysulfide system.

Figure 3(e) presents the total thermal conductivity κ and the lattice thermal conductivity κ_L of all samples. The κ of the parent compound exhibits a weak temperature dependence, increasing modestly from 0.98 W m^{-1} K^{-1} at 300 K to 1.05 W m^{-1} K^{-1} at 773 K. This slight upturn is dominated by the electronic contribution in the degenerate n-type semiconductor, calculated by $\kappa_e = LT/\rho$ with a degenerate Lorenz number $L = 2.44 \times 10^{-8}$ W Ω K^{-2}. For the compensated samples ($x = 0.02, 0.04$), κ is systematically lower across the entire temperature range due to their reduced electrical conductivity, which suppresses κ_e. In contrast, the heavily doped p-type samples ($x = 0.06, 0.08$) exhibit significantly higher κ values and a more pronounced temperature dependence, reaching 1.29–1.38 W m^{-1} K^{-1} at 773 K. The enhancement is a direct consequence of the high electrical conductivity, which leads to a large electronic thermal conductivity. The lattice thermal conductivity κ_L, obtained by subtracting the electronic contribution, is also shown. The parent compound exhibits a κ_L of 0.86 W m^{-1} K^{-1} at 300 K, comparable to that of layered LaOBiSSe[6], indicating that low κ_L is a characteristic feature of this layered oxysulfide system. Upon Na doping, κ_L decreases monotonically at 300 K from 0.78 W m^{-1} K^{-1} (x = 0.02) to 0.48 W m^{-1} K^{-1} (x = 0.08). This reduction in κ_L is consistent with enhanced phonon scattering by the mass and strain-field fluctuations associated with Na substitution on the Pb site[19], as also observed in Na-doped layered oxychalcogenides such as BiCuSeO[20], which partially

offsets the increase in κ_e for the heavily doped p-type samples. Despite the increase in total thermal conductivity for the p-type samples, the overall thermal conductivity of this layered system remains relatively low, which provides a favorable basis for achieving promising thermoelectric performance.

To assess the potential influence of residual porosity on the measured properties, we refer to the effective medium theory (EMT) for porous thermoelectric materials. For a porosity of ∼8% (relative density ∼92%), the Maxwell–Eucken model, which applies to a dilute dispersion of isolated, near-spherical, and non-interconnected pores ($p \lesssim 10\%$)[21], predicts that the effective electrical conductivity ($\sigma = 1/\rho$) and thermal conductivity are reduced by approximately 11–12% relative to the fully dense values. In contrast, the Seebeck coefficient is largely insensitive to porosity because the pores are electrically insulating and do not contribute to the thermopower. Consequently, the power factor may be underestimated by ∼12%, while ZT is nearly invariant; any additional phonon scattering by the residual pores would only lower κ, making the estimate conservative. It should be noted that all samples exhibited comparable relative densities within 91–93%, ensuring that the compositional trends reported here are not significantly biased by porosity variation.

The dimensionless figure of merit ZT is presented in Fig. 3(f). The parent sample exhibits a modest ZT of 0.13 at 773 K, limited by its low power factor. The compensated samples ($x = 0.02, 0.04$) show similarly poor performance. Upon entering the p-type regime, a remarkable enhancement of ZT is observed: the $x = 0.06$ sample achieves a maximum ZT of 0.33 at 773 K, while the x = 0.08 sample reaches 0.29. The slightly lower ZT of $x = 0.08$ is a consequence of the high-temperature resistivity anomaly and reduced Seebeck coefficient, both stemming from the over-doping effect.

The non-monotonic behavior of the electrical transport properties with Na content reveals a more intricate doping mechanism than a simple rigid-band picture would predict. In the heavily doped p-type regime ($x = 0.08$), the simultaneous anomaly in resistivity and Seebeck coefficient above 600 K suggests a temperature-induced modification of the electronic structure. However, the present data alone cannot unambiguously identify the dominant mechanism. One plausible scenario is that at elevated temperatures, the Fermi level shifts closer to the mid-gap region due to the thermal activation of minority electrons, leading to a mixed carrier conduction state[22]. Alternatively, the high concentration of Na^+ ions at the Pb^{2+} site may introduce local lattice strain, triggering a subtle structural modulation

that transiently enhances carrier scattering[23, 24]. It is worth noting that strain-induced changes in the local density of states and the effective mass near the Fermi level can also modify the Seebeck coefficient, not merely the scattering rate[25]. In addition, the total thermal conductivity exhibits a discernible anomaly in the same temperature range (Fig. 3e), which may arise from strain-induced modifications of phonon scattering. The presence of a minor Na_2S impurity phase in the $x = 0.08$ sample further complicates the interpretation. Since Na_2S is electrically insulating and present only in small amounts, it is unlikely to be the sole origin of the pronounced anomaly in both resistivity and Seebeck coefficient. A more plausible explanation is that the anomaly arises from the combined effects of bipolar conduction, strain-induced scattering, and the minor Na_2S impurity phase, which together account for the observed resistivity hump and the accompanying Seebeck anomaly while also limiting the ZT of the over-doped sample. Further microscopic investigations, such as high-temperature synchrotron X-ray diffraction and pair distribution function analysis, would be valuable to clarify the structural evolution underlying these transport anomalies.

IV. CONCLUSION

In summary, we have demonstrated that Na substitution at the Pb site in the layered oxysulfide $LaOBiPbS_3$ enables systematic control of both the type and density of charge carriers, achieving a complete carrier-type conversion from intrinsic n-type to p-type conduction. A well-defined compensation point is established near $x = 0.04$, beyond which the system enters a degenerate p-type regime. The optimal composition $LaOBiPb_{0.94}Na_{0.06}S_3$ delivers a maximum power factor of 5.45 $\mu W\,cm^{-1}\,K^{-2}$ and a peak ZT of 0.33 at 773 K, reaching 3.2 and 2.5 times the PF and ZT values of the parent compound, respectively. Pisarenko analysis confirms that Na doping primarily modulates the carrier concentration without significantly altering the density-of-states effective mass near the Fermi level. For the over-doped $x = 0.08$ sample, a high-temperature anomaly in both resistivity and Seebeck coefficient is observed above 600 K, tentatively attributed to the interplay of bipolar conduction and local lattice strain induced by excessive Na incorporation. The present results demonstrate that Na doping is an effective route to realizing p-type thermoelectricity in the layered oxysulfide $LaOBiPbS_3$, with further performance enhancement anticipated through targeted band and phonon engineering.

V. ACKNOWLEDGMENTS

This work was financially supported by the National Natural Science Foundation of China (NSFC) (Grants Nos. 51572001, 11404002, and 11404003), the University Natural Science Research Project of Anhui Province (Grant No. KJ2019A0019), and the Natural Science Foundation of Anhui Province (Grant No. 2008085QA42).

[1] Wang J, Yin Y G, Che C W and Cui M Y 2025 *Energies* **18** 2122

[2] Zachariah S and Ravanan I 2025 *J. Alloys Compd.* **1043** 184187

[3] Mizuguchi Y, Omachi A, Goto Y, Kamihara Y, Matoba M, Hiroi T, Kajitani J and Miura O 2014 *J. Appl. Phys.* **116** 163915

[4] Guo K, Wang X Q, Huang H, Yu X T, Zeng Y Q, Lin J Y, Hu X Q, Li S K, Li H and Zhao J T 2023 *J. Alloys Compd.* **947** 169601

[5] Shahid O, Srivastava K and Prakash J 2026 *Mater. Sci. Eng. B* **324** 118995

[6] Nishida A, Miura O, Lee C H and Mizuguchi Y 2015 *Appl. Phys. Express* **8** 111801

[7] Omachi A, Kajitani J, Hiroi T, Miura O and Mizuguchi Y 2014 *J. Appl. Phys.* **115** 083909

[8] Sun Y L, Ablimit A, Zhai H F, Bao J K, Tang Z T, Wang X B, Wang N L, Feng C M and Cao G H 2014 *Inorg. Chem.* **53** 11125–11129

[9] Mizuguchi Y, Hijikata Y, Abe T, Moriyoshi C, Kuroiwa Y, Goto Y, Miura A, Lee S, Torii S, Kamiyama T, Lee C H, Ochi M and Kuroki K 2017 *Europhys. Lett.* **119** 26002

[10] Kurematsu K, Ochi M, Usui H and Kuroki K 2020 *J. Phys. Soc. Jpn.* **89** 024702

[11] Yu Y, Wang C C, Li Q J, Cheng C, Wang S T and Zhang C J 2019 *Ceram. Int.* **45** 817–821

[12] Hijikata Y, Abe T, Moriyoshi C, Kuroiwa Y, Goto Y, Miura A, Tadanaga K, Wang Y, Miura O and Mizuguchi Y 2017 *J. Phys. Soc. Jpn.* **86** 124802

[13] Zhao L D, He J, Wu C I, Hogan T P, Zhou X, Uher C, Dravid V P and Kanatzidis M G 2012 *J. Am. Chem. Soc.* **134** 7902

[14] Zhao X W, Fu B Q and Ang R 2024 *Adv. Funct. Mater.* **34** 2401582

[15] Yu L, Yu H, Chen L C, Pang H J, Zhang Q, Ren Z F and Chen X J 2025 *Phys. Rev. B* **112** 214302

[16] Grovogui J A, Slade T J, Hao S, Wolverton C, Kanatzidis M G and Dravid V P 2021 *J. Mater.*

Res. **36** 1272

[17] Roux-Byl C and Berardan D 2021 *J. Mater. Chem. C* **9** 12839–12848

[18] Nayak S and Nagaraja K K 2020 *J. Alloys Compd.* **814** 152137

[19] Klemens P G 1955 *Proc. Phys. Soc. A* **68** 1113–1128

[20] Li J, Sui J, Pei Y L, Meng X F, Berardan D, Dragoe N, Cai W and Zhao L D 2014 *J. Mater. Chem. A* **2** 4903–4906

[21] Sevostianov I, Mogilevskaya SG and Kushch VI 2019 *Int. J. Eng. Sci.* **140** 35–88

[22] Wang D Z, You C, Ge Y F, Wang F, Wang X L, Liang X, Zhou Q, Tao Q, Chen Y L and Zhu P W 2024 *Appl. Phys. Lett.* **125** 013903

[23] Jang H, Park J H, Lee H S, Ryu B, Park S D, Ju H A, Yang S H, Kim Y M, Nam W H, Wang H, Male J, Snyder G J, Kim M, Jung Y S and Oh M W 2021 *Adv. Sci.* **8** 2100895

[24] Wang L K, Zhu J B, Dong X Y, Zhu Y K, Jiao L, Xia B Y, Zhou J W, Guo F K, Bordelon M, Wilson S D, Cai W, Sui J H and Liu Z H 2025 *Appl. Phys. Rev.* **12** 011417

[25] Heremans JP, Jovovic V, Toberer ES, Saramat A, Kurosaki K, Charoenphakdee A, Yamanaka S and Snyder GJ 2008 *Science* **321** 554–557